SCIENCE CHINA
Chemistry

•ARTICLES•

October 2021 Vol.64 No.10: 1786–1795
https://doi.org/10.1007/s11426-021-1096-8

Intermolecular charge-transfer aggregates enable high-efficiency near-infrared emissions by nonadiabatic coupling suppression

Jie Xue[1,2], Jingyi Xu[1], Jiajun Ren[1*], Qingxin Liang[1], Qi Ou[1], Rui Wang[1], Zhigang Shuai[1] & Juan Qiao[1,2*]

[1]*Key Lab of Organic Optoelectronics and Molecular Engineering of Ministry of Education, Department of Chemistry, Tsinghua University, Beijing 100084, China;*
[2]*Center for Flexible Electronics Technology, Tsinghua University, Beijing 100084, China*

Received May 27, 2021; accepted August 16, 2021; published online August 30, 2021

Pursuing purely organic materials with high-efficiency near-infrared (NIR) emissions is fundamentally limited by the large non-radiative decay rates (k_{nr}) governed by the energy gap law. To date, reported endeavors to decelerate k_{nr} are mainly focused on reducing the electron-vibration coupling with the electronic nonadiabatic coupling assumed as a constant. Here, we demonstrated a feasible and innovative strategy by employing intermolecular charge-transfer (CT) aggregates (CTA) to realize high-efficiency NIR emissions *via* nonadiabatic coupling suppression. The formation of CTA engenders intermolecular CT in the excited states; thereby, not only reducing the electronic nonadiabatic coupling and contributing to small k_{nr} for high-efficiency NIR photoluminescence, but also stabilizing excited-state energies and achieving thermally activated delayed fluorescence for high-efficiency NIR electroluminescence. This work provides new insights into aggregates and opens a new avenue for organic materials to overcome the energy gap law and achieve high-efficiency NIR emissions.

nonadiabatic coupling, intermolecular charge-transfer, molecular aggregates, organic light-emitting diodes, thermally activated delayed fluorescence

Citation: Xue J, Xu J, Ren J, Liang Q, Ou Q, Wang R, Shuai Z, Qiao J. Intermolecular charge-transfer aggregates enable high-efficiency near-infrared emissions by nonadiabatic coupling suppression. *Sci China Chem*, 2021, 64: 1786–1795, https://doi.org/10.1007/s11426-021-1096-8

1 Introduction

Harnessing the near-infrared (NIR) light is of great importance for optogenetics, phototherapy, bio-imaging, medical diagnosis and optical communications [1–5]. In recent years, NIR organic materials have attracted rapidly growing interest because of their potential as efficient, low-toxic, low-cost and even disposable NIR photosensitizers and light sources [3,4]. Particularly, the inherent flexibility of organic materials has accelerated the development of NIR organic light-emitting diodes (OLEDs) as flexible, wearable and implantable devices [4,6–9]. Extending π-conjugation length and employing donor-acceptor charge transfer states have proven to be effective molecular design strategies to realize NIR emissions [3]. However, these conventional NIR organic molecules usually suffer from large non-radiative decay rates (k_{nr}) and low photoluminescence (PL) quantum yields (PLQY) due to the energy gap law [4,10,11], which dictates accelerated non-radiative processes from the lowest excited state (S_1) to ground state (S_0) caused by molecular vibrations as the optical energy gap falls towards deep-red and NIR region. Therefore, high-efficiency NIR-OLEDs are still rare, even though great breakthroughs have been made for purely organic materials to harvest the weakly emissive triplet excitons generated by electroexcitation [12–15].

To alleviate the limitation imposed by the energy gap law,

*Corresponding authors (email: qjuan@mail.tsinghua.edu.cn; renjj@tsinghua.edu.cn)

considerable efforts have been made for organic materials to decelerate the non-radiative decay processes by reducing the electron-vibration coupling. At the single-molecule level, employing rigid molecular structure can hinder low-frequency vibrations in molecules, and perdeuterated or perfluorinated approaches can alleviate high-frequency vibrations [16–18]. Nevertheless, these strategies would inevitably increase the difficulty and cost of the synthesis. Beyond the single-molecule level, the advances in understanding the aggregation effect on organic luminescence indicate that intermolecular packing sometimes can hinder the non-radiative decay processes caused by low-frequency vibrations of functional groups [19,20]. However, there is still a large room for the improvement of the luminescence efficiency of NIR organic materials, which requires deeper insights into the energy gap law.

In this work, from a fundamental perspective on the energy gap law, we found the suppression of electronic nonadiabatic coupling is a novel approach for organic emissive materials to decelerate the non-radiative decay processes and overcome the energy gap law. Furthermore, we demonstrated a feasible strategy by employing intermolecular charge-transfer (CT) aggregates (CTA) to suppress the nonadiabatic coupling and achieve high-efficiency NIR emissions. The formation of CTA with the involvement of intermolecular CT (xCT) in the excited states can not only reduce the nonadiabatic coupling, which leads to a small k_{nr} for high-efficiency NIR photoluminescence, but also stabilize excited-state energies, which induces strong thermally activated delayed fluorescence (TADF) for high-efficiency NIR electroluminescence (EL). The developed purely organic CTA emitter exhibited widely-tunable emissions from 621 to 802 nm with high PLQYs of over 80% in NIR region and high maximum external-quantum-efficiencies (EQEs) of 17.0% in NIR-OLEDs.

2 Results and discussion

2.1 Theoretical analysis and conceptual design

First, we briefly review the theoretical background of the non-radiative decay rate k_{nr}. For organic molecules in the weak coupling limit (Huang-Rhys factor S_i<<1), k_{nr} can be expressed as [11]:

$$k_{nr} = \sum_l C_l^2 \frac{\sqrt{2\pi}}{\sqrt{\omega_M \Delta E}} \exp\left(-\sum_i S_i\right) \exp\left\{-\frac{\Delta E}{\omega_M}\left[\ln\left(\frac{\Delta E}{\lambda_M}\right) - 1\right]\right\} \quad (1)$$

The prefactor C_l^2 is related to the nonadiabatic coupling elements (NACE) between the ground state φ_{gs} and the excited state φ_{ex} along mode l, which is called the promoting mode triggering the electronic transition.

$$C_l^2 = \left| \left\langle \varphi_{ex} \left| \frac{\partial}{\partial q_l} \right| \varphi_{gs} \right\rangle \right|^2 \frac{\omega_l}{2} \quad (2)$$

The other parts of Eq. (1) are related to the Franck-Condon factor-weighted density of states, *i.e.*, the overlap between the initial and final vibrational wavefunctions, which represents the ability of vibrations to receive the electronic energy. ω_M is the frequency of the normal vibrations of maximum frequency. λ_M is the total reorganization energy of the vibrations with the frequency ω_M. ΔE is the adiabatic energy gap between the electronic ground and excited states. Commonly, it is believed that k_{nr} would increase exponentially with the decrease of ΔE under the assumption that the prefactor C_l^2 is unchanged. This is the widely known energy gap law which mainly hinders the development of high-efficiency NIR materials.

From Eq. (1), it is clear that the k_{nr} of organic molecules is determined by two factors, the electronic nonadiabatic coupling and the Franck-Condon factor-weighted density of states. To date, the strategies to reduce k_{nr} of organic materials are mainly focused on suppressing the second part of Eq. (1) by reducing λ_M and ω_M [16−22]. Notably, Zhou and Chi *et al.* [22] proposed that exciton delocalization in well-aligned Pt(II) complexes could reduce the reorganization energy λ_M and achieve high-efficiency NIR-OLEDs. Besides the suppression of electron-vibration coupling, the reduction of electronic nonadiabatic coupling is another approach to reduce k_{nr} and overcome the energy gap law. However, the prefactor C_l^2 corresponding to the electronic NACE is commonly assumed as a constant and its effect is rarely discussed. Within the complete basis set limit [23], the NACE is qualitatively proportional to the electronic transition density, determined by the overlap between the electron and hole wavefunctions as shown in Eqs. (3) and (4):

$$\left\langle \varphi_{ex} \left| \frac{\partial}{\partial q_l} \right| \varphi_{gs} \right\rangle \approx \frac{1}{E_{ex} - E_{gs}} \sum_\sigma \frac{Z_\sigma e^2}{\sqrt{M_\sigma}} \sum_{i=x,y,z} E_{\sigma i} L_{\sigma i,l} \quad (3)$$

$$E_{\sigma i} = \int \mathrm{d}\vec{r} \rho(\vec{r}) \frac{e(r_i - R_{\sigma i})}{\left|\vec{r} - \vec{R}_\sigma\right|^3} \approx \int \mathrm{d}\vec{r} \phi_{elec}(\vec{r}) \phi_{hole}(\vec{r}) \frac{e(r_i - R_{\sigma i})}{\left|\vec{r} - \vec{R}_\sigma\right|^3} \quad (4)$$

where $L_{\sigma i,l}$ is the transformation matrix between the normal coordinates and Cartesian coordinates and $E_{\sigma i}$ is atomic electric field experienced by the overlap of electrons and holes from the excited state. From Eqs. (1–4), we propose that the decrease of the overlap of electrons and holes in the excited states can reduce the prefactor C_l^2, thus suppressing the non-radiative decay processes for a small k_{nr}.

2.2 Molecular design and synthesis

Recently, we found the formation of J-aggregates with strong xCT can significantly stabilize the excited-state energies of organic materials, thus inducing and enhancing highly effi-

cient TADF [24]. Most importantly, the formation of such molecular aggregates can lead to a decreased k_{nr} with the decrease of the optical energy gap, totally deviating from the exponential increase trend imposed by the energy gap law [24]. Although the underlying mechanism was unclear at that time, it could benefit from the nonadiabatic coupling suppression induced by xCT with the larger separation of electrons and holes than that of intramolecular CT (iCT). To illustrate the underlying mechanism and achieve high-efficiency NIR emissions, the molecule dpTPAAP (Figure 1) for CTA was designed based on the reported TPAAP with the same electron acceptor acenaphtho[1,2-*b*]pyrazine-8,9-dicarbonitrile (AP) and modified electron donor bis(biphenyl-4-yl)phenylamine (dpTPA) [24]. The addition of phenyl groups could increase the delocalization of the highest occupied molecular orbital (HOMO), which would be conducive to red-shifted emission with a high PLQY [25,26]. And the similar donor-acceptor framework could endow dpTPAAP with strong xCT in aggregation states to construct CTA for NIR emission. For comparison, an iCT molecule with similar molecular framework, dpTPAAZ, was designed by fusing electron acceptor pyrazine on the acceptor moiety of dpTPAAP to enhance the iCT and realize NIR emission at the single-molecule level. The fusion of rigid pyrazine could maintain the molecular rigidity, thus reducing the extra non-radiative decay processes as much as possible. The comparative investigations on photophysical behaviors of CTA and commonly-used iCT molecules were conducted to uncover the distinct underlying mechanism and explore the rational design of high-efficiency NIR organic materials.

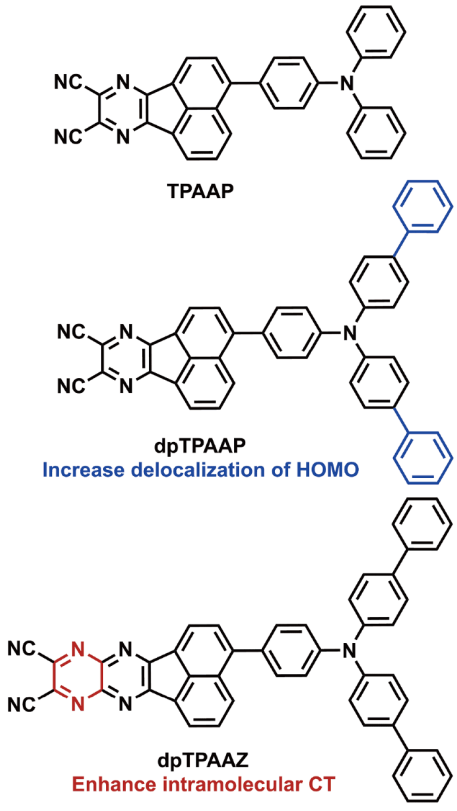

Figure 1 Design strategies for organic NIR emitters and chemical structures of dpTPAAP and dpTPAAZ (color online).

Both dpTPAAP and dpTPAAZ were synthesized in three steps involving bromination, Suzuki-Miyaura cross-coupling reaction and dehydration cyclization reaction. These new compounds were characterized by nuclear magnetic resonance (NMR) spectroscopy, high-resolution mass spectrometry, and elemental analysis. Thermogravimetric analysis (TGA) measurements revealed that both dpTPAAP and dpTPAAZ have high decomposition temperatures (T_d, corresponding to 5% weight loss) at 414 and 498 °C, respectively.

2.3 Single crystal and molecular packing

During temperature-gradient vacuum sublimation, single crystalline dpTPAAP were readily obtained. The molecular structure and packing motifs of dpTPAAP in crystalline states were identified by single-crystal X-ray crystallographic analysis. The dpTPAAP molecules possess relatively planar structures and the dihedral angle between donor and acceptor subunits is 33° (Figure 2a). In crystalline state, the nearest neighbouring dpTPAAP molecules form dimers in a face-to-face fashion (Figure 2b) with the donor of one molecule close to the acceptor of the other molecule, which is supported by intermolecular CN···H−C interactions with a distance of 2.886 Å and intermolecular π···π interactions with a distance of 3.521 Å between the AP acceptor cores. These head-to-tail dimers pack up in a herringbone arrangement in the crystal (Figure 2c), which is much different from the staircase packing mode of its counterpart TPAAP [24].

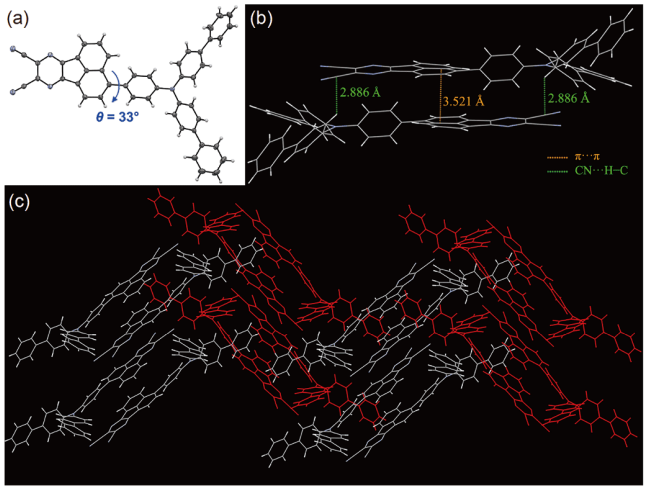

Figure 2 (a) Single-crystal structure of dpTPAAP with thermal ellipsoids plotted at 50% probability level. (b) Packing motifs of aggregated dimers. (c) Packing motifs of dpTPAAP in single crystals (color online).

2.4 Photophysical properties

To study the photophysical properties of these compounds as single molecules, oxygen-free dilute toluene solutions (1×10^{-5} mol L^{-1}) of dpTPAAP and dpTPAAZ were prepared. As shown in Figure 3a, the intense absorption bands below 430 nm are assigned to the localized π–π* transitions and the moderate absorption bands over 430 nm are ascribed to the iCT transitions. The broad iCT absorption band of dpTPAAZ can be deconvoluted (Gaussian multi-peak fitting) into two absorption bands (Figure S2); the high-energy band with peak at 466 nm corresponds to the second lowest excited single state (S_2), and the low-energy band with peak at 538 nm corresponds to S_1, which is red-shifted compared with that of dpTPAAP with the peak at 501 nm due to the enhancement of iCT. Under photoexcitation, dpTPAAP displays intense red fluorescence (λ_{max} = 624 nm) with a high PLQY of up to 97.4% and a short lifetime of 7.94 ns (Figure S3). The remarkable PLQY results from high k_r value of 1.2×10^8 s^{-1} and low k_{nr} value of 3.3×10^6 s^{-1}. As expected, thanks to the enhancement of iCT, dpTPAAZ exhibits largely red-shifted emission into desired NIR region (λ_{max} = 763 nm) in toluene solution. Unfortunately, such large red-shift of the emission leads to a dramatically reduced PLQY to 7.6%. The low PLQY of dpTPAAZ results from the low k_r value of 1.8×10^7 s^{-1} and high k_{nr} value of 2.2×10^8 s^{-1}. In comparison with dpTPAAP, dpTPAAZ showed almost one order of magnitude smaller k_r value and two orders of magnitude larger k_{nr} value,

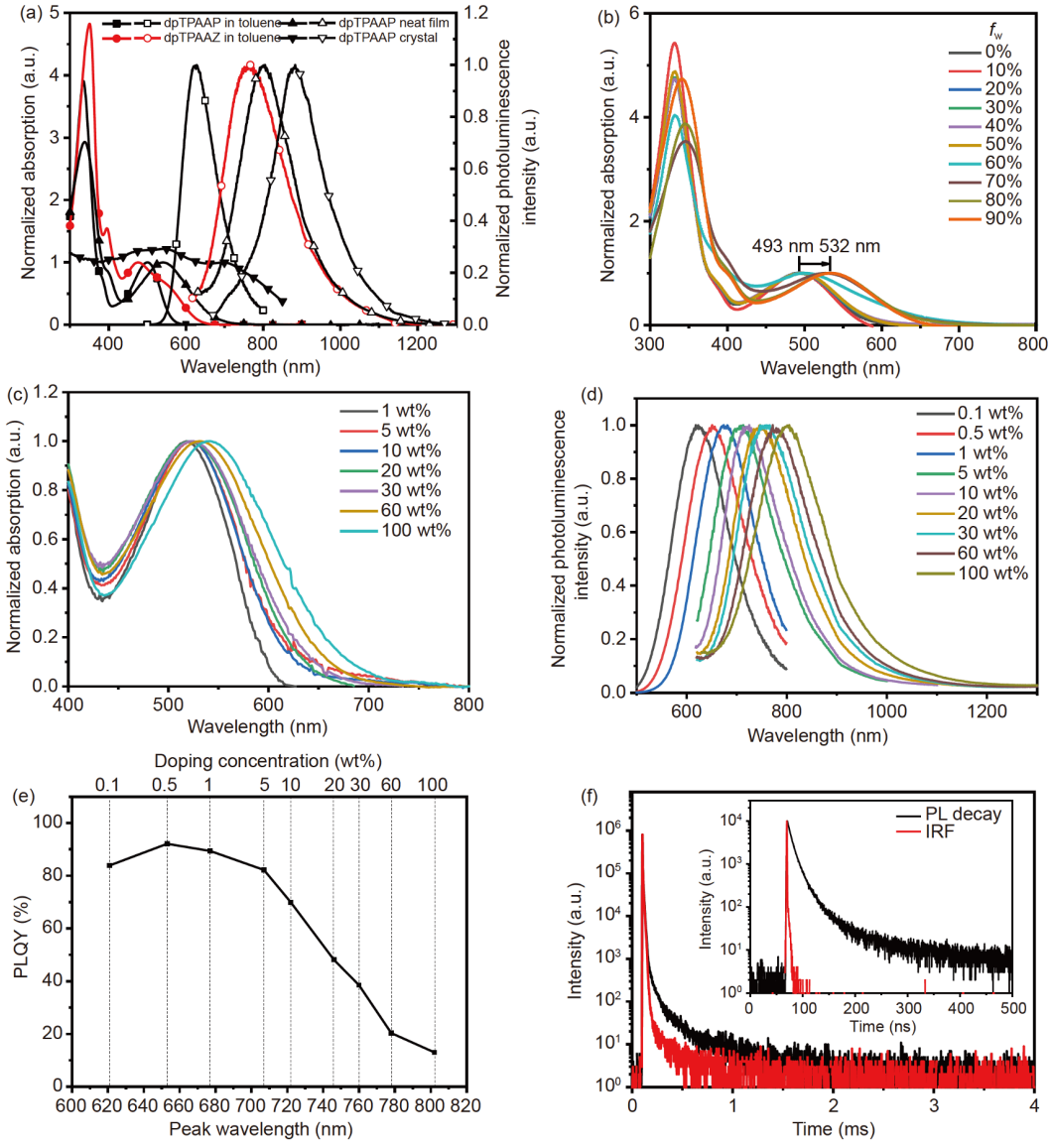

Figure 3 (a) Absorption (solid symbol) and PL (open symbol) spectra of dpTPAAP and dpTPAAZ in toluene (1×10^{-5} mol L^{-1}), dpTPAAP in neat films and single crystals. (b) Absorption spectra of dpTPAAP in THF/water mixtures (1×10^{-5} mol L^{-1}) with different water fractions (f_w). (c) Absorption spectra, (d) PL spectra and (e) PLQY of dpTPAAP in solid films with TPBi as a host at various doping concentrations at room temperature. (f) Transient PL decay curves of 30 wt.% dpTPAAP:TPBi films. Inset: the prompt decay curves in nanosecond scale (color online).

clearly manifesting that the photophysical behaviours of single organic molecule are severely limited by the energy gap law.

In addition to enhancing iCT at the level of single molecule, the formation of aggregates with strong xCT could also achieve desired red-shift of emission [24,27,28]. In the neat film, dpTPAAP shows desired NIR emission (λ_{max} = 802 nm), with a 178 nm red-shift compared with that in toluene solution. The neat film gives a remarkable PLQY of 13.0%, which is three times higher than that of the curcuminoid derivative reported by Adachi *et al.* [29] (λ_{max} = 801 nm and PLQY = 4%). Also, the CT absorption band of the neat film shows a substantial red-shift (~40 nm) with corresponding peak wavelength located at 541 nm, which indicates the formation of molecular aggregates with strong xCT [24]. The single crystals of dpTPAAP demonstrated further red-shifted absorption and emission (λ_{max} = 882 nm) compared with its neat film (Figure 3a), suggesting a more significant xCT in single crystals. Importantly, the dpTPAAP single crystal shows a good PLQY of 4.4%.

To investigate the influences of molecular aggregation and environmental dipole on exciton states of dpTPAAP, we measured the absorption spectra of dpTPAAP in tetrahydrofuran (THF)/water mixtures with different water volume fractions (f_w). As shown in Figure 3b, although the polarity of THF/water mixture rises as the increase of f_w from 0% to 50%, the absorption spectra of dpTPAAP are almost unchanged, thus excluding the possibility of environmental dipole-induced large red-shift of absorption. The further increase of f_w from 50% leads to an abrupt red-shift of CT absorption bands accompanied by the formation of nanoparticles with the peak finally pinned at 532 nm, manifesting that the formation of molecular aggregates is the main cause for the large red-shift of CT absorption bands, which greatly stabilizes the exciton states.

To explore the evolution of molecular aggregates in solid states, we studied the photophysical properties of doped films with dpTPAAP in 2,2′,2″-(1,3,5-benzinetriyl)-tris(1-phenyl-1-*H*-benzimidazole) (TPBi) at different doping concentrations. As shown in Figure 3c, the absorption spectra of the doped films show progressive red-shift with increasing doping concentration, manifesting the gradual formation of molecular aggregates. Meanwhile, these films demonstrate widely-tunable PL by simply controlling the doping concentration (Figure 3d, e). At very low doping concentration of 0.1 wt.%, the doped film displays strong red PL (λ_{max} = 621 nm), which is similar to the PL of dpTPAAP in dilute toluene solutions. As the increase of doping concentration, the 0.5 wt.% and 1 wt.% doped film give strong deep-red (DR) emissions at 653 nm and 677 nm with very high PLQYs of 92.1% and 89.4%, respectively. When doping concentration increases to 5 wt.%, the doped film displays a desired NIR emission (λ_{max} = 707 nm) with a high PLQY of 82.2%. The doped films show persistently red-shifted PL as the doping concentration continuously increases.

Notably, the desired NIR PL with peak wavelength at 760 nm is realized in the 30 wt.%-doped film, which is almost the same as the PL (λ_{max} = 763 nm) of dpTPAAZ molecules in toluene. Moreover, the 30 wt.%-doped film has an impressive PLQY of up to 38.5%, which is 5 times higher than that of dpTPAAZ molecules in toluene. Such remarkable PLQY benefits from its high k_r value of 2.26×10^7 s^{-1} and low k_{nr} value of 3.60×10^7 s^{-1}. The k_r value is 1.2 times higher than that of dpTPAAZ molecules in toluene, which indicates that the formation of such molecular aggregates is favourable to obtain high k_r values. Importantly, the film displays a substantially reduced k_{nr} value by about one order of magnitude compared with that of dpTPAAZ molecules in oxygen-free toluene. This demonstrates that the formation of CTA could significantly suppress the non-radiative decay processes and contribute to a small k_{nr} value rather than a rapid increased k_{nr} value according to the energy gap law. Meanwhile, the 30 wt.%-doped film exhibits prominent TADF consisting of a nanosecond-scale prompt component (average lifetime τ_p = 16.3 ns) and a microsecond-scale delayed component (average lifetime τ_{TADF} = 39.4 μs) at room temperature (Figure 3f and Figure S6), which could be ascribed to the substantially reduced energy gap (ΔE_{ST}) between the S_1 and lowest triplet (T_1) excited state of only 0.073 eV as the result of molecular aggregation and the self-polarization-induced solid-state solvation effect [24,30].

The photophysical properties of dpTPAAZ in the doped films were also studied for comparison. The 5 wt.%-doped dpTPAAZ:TPBi film displays NIR emission with peak wavelength at 764 nm (Figure S7) and a low PLQY of 5.9%, which are close to those of dpTPAAZ molecules in toluene (λ_{max} = 763 nm, PLQY = 7.6%). From dilute toluene solution to 5 wt.%-doped film, the k_{nr} value of dpTPAAZ reduces from 2.2×10^8 to 1.4×10^8 s^{-1}, which could be ascribed to the suppression of low-frequency molecular motions in solid state. Remarkably, the 30 wt.%-doped dpTPAAP:TPBi film has almost the same emission (λ_{max} = 760 nm) as that of the 5 wt.%-doped dpTPAAZ:TPBi film, but its k_{nr} value is less than one third of the latter's. In general, the doped films with high doping concentration would exhibit large k_{nr} caused by aggregation-caused quenching. The unexpected low k_{nr} value of the 30 wt.%-doped dpTPAAP:TPBi film could benefit from the formation of CTA. Consequently, the PLQY of the 30 wt.%-doped dpTPAAP:TPBi film is 6.5 times higher than that of the 5 wt.%-doped dpTPAAZ:TPBi film.

2.5 Electron paramagnetic resonance

To investigate the xCT in the aggregation states, we performed electron paramagnetic resonance (EPR) measurements on the single crystals and the neat film of dpTPAAP.

As shown in Figure 4a, the single crystals of dpTPAAP under dark condition displayed clear EPR signals with the *g*-factor determined to be 2.0033. Under photoexcitation, its EPR signal is slightly enhanced. Unlike the single crystal with a long-range order, the neat film of dpTPAAP is more likely to be amorphous (Figure S9). Nevertheless, the neat film of dpTPAAP also displayed EPR signals under dark condition with the *g*-factor determined to be 2.0040 (Figure 4b). Under photoexcitation, its EPR signal is remarkably enhanced instead. Both the *g*-factors of EPR signals of the single crystals and the neat film are close to the value of free electron (2.0023), indicating the presence of unpaired electrons. Since dpTPAAP is a closed-shell neutral molecule, the unpaired electrons could be ascribed to the charged ions generated by xCT in the ground state due to the formation of CTA [27,31]. The significantly enhanced EPR signal of the neat film under photoexcitation demonstrates that more charged ions are generated by xCT under photoexcitation, which clearly highlights the xCT nature in the excited states. For comparison, the photoexcitation only led to a slightly enhanced EPR signal for dpTPAAP single crystals, which could be ascribed to the opacity of single crystals that allows only a small ratio of molecules photoexcited under illumination.

2.6 Quantum chemical calculations

To understand the photophysical behaviours of dpTPAAP, we carried out theoretical investigations on the electronic structures of monomers and dimers in the gas phase using density-functional theory (DFT) and time-dependent DFT (TDDFT). An optimal tuning version of ωB97XD long-range corrected functional (ω = 0.1264) was used to describe the CT excited states [32]. The S_1 and T_1 energies of the monomer at the optimized S_0 geometry were calculated to be 2.89 and 2.20 eV, respectively. According to the analysis of attachment (electron)/detachment (hole) density and fragment-based transition density matrices (TDM) of S_1 and T_1 states calculated by the Q-Chem and Multiwfn 3.7 package [33–35], the S_1 state of the monomer is predominantly an iCT state from the donor fragment to the acceptor fragment, while the T_1 state is mainly a local excitation state in the acceptor fragment (Figure 5a, b).

To investigate the aggregation effect on the electronic structure, we extracted 14 nearest-neighbour dimers from the single crystal (Figure S11). Among them, dimer **1** with a face-to-face stacking leads to the most significant reductions of S_1 and T_1 energies (Table S4), and the S_1 and T_1 energies are 2.31 and 1.95 eV, respectively, at the optimized S_0 geometry. The S_1 and T_1 energies of other dimer are close to those of monomers. Figure 5c shows that, unlike the case of monomers, the S_1 state of dimer **1** is mainly composed of xCT and mixed with a small iCT component. On the contrary, the T_1 state maintains the local excitation feature of monomers and is mixed with a small xCT component. This different contributions of xCT components into S_1 and T_1 states result in a different amount of reduction of S_1 and T_1 energies upon aggregation (ΔE_{S1} = 0.58 eV, ΔE_{T1} = 0.25 eV). Therefore, the singlet-triplet gap decreases in favour of TADF in the solid phase.

Apart from the contribution of xCT, the excitonic coupling is another possible effect to account for the aggregation-induced spectrum shift. After Boys-localized diabatization carried out in the developmental version of Q-Chem within the lowest 4 singlet excited states (Figure 5d), it is clear to see that they are composed of 2-degenerate low-energy pure xCT states and 2-degenerate high-energy pure iCT states. The large electronic coupling, $\langle xCT_1|H|iCT_2\rangle = \langle xCT_2|H|iCT_1\rangle$ = −103 meV, may help the weakly emitting xCT state borrow the oscillator strength from the iCT state to enhance k_r if the ideal degeneracy is broken with static disorder in the real film. However, the excitonic coupling between the iCT states is only 26 meV, which has a minor effect on the S_1 state of the dimer **1**.

The introduction of xCT components into the excited states not only reduces the excitation energy, but also reduces NACE, which is essential to the high-efficiency NIR luminescence. In CTA, we found that the reduction of NACE played a major role in suppressing non-radiative decay

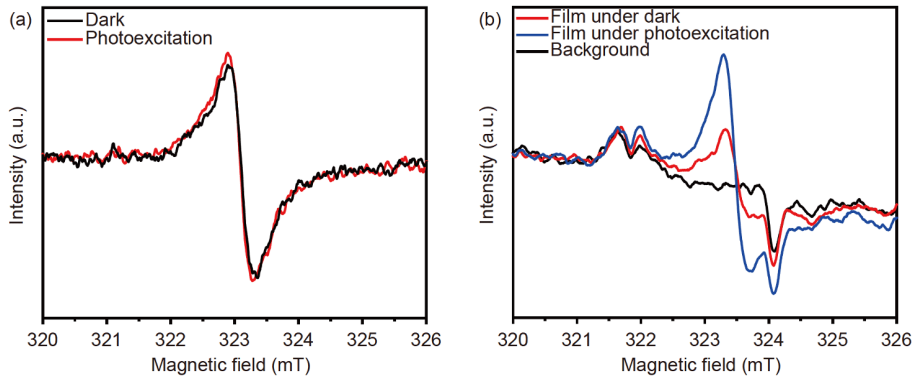

Figure 4 EPR signals of dpTPAAP (a) single crystals and (b) neat films under dark condition and photoexcitation (color online).

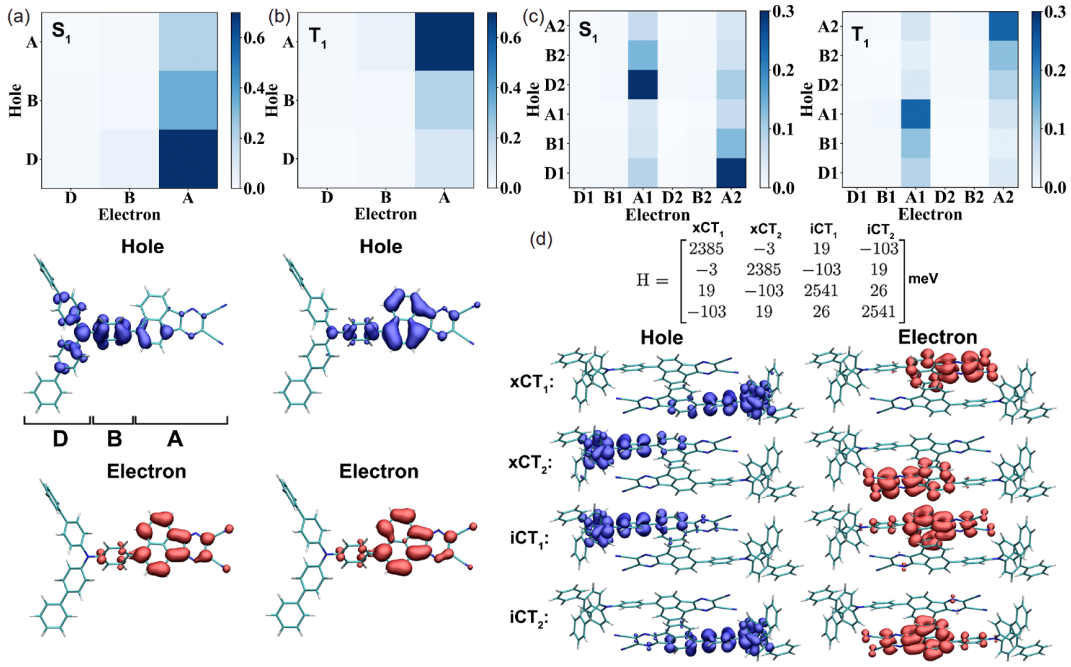

Figure 5 Fragment-based TDM (D/B/A denotes donor/bridge/acceptor) and attachment (electron)/detachment (hole) density (isovalue = 0.001) for (a) S_1 and (b) T_1 states of dpTPAAP monomers. (c) TDM for S_1/T_1 states of dpTPAAP dimer **1**. (d) The diabatic Hamiltonian and electron/hole density of the lowest 4 diabatic states (2 xCT and 2 iCT) of dpTPAAP dimer **1** (color online).

process when the S_1 state changed from iCT to xCT upon aggregation. In Figure 6, C_l in Eq. (1) for different promoting modes of the dpTPAAP monomer and dimer **1** is shown. For the monomer, the modes between 1,300 and 1,600 cm^{-1}, typically corresponding to the high-frequency stretching vibrations of skeleton bonds, most contribute to the prefactor. By contrast, for dimer **1**, C_l in the same frequency window is largely suppressed. The largest component decreases from 40 to 15 cm^{-1}. This reduction is due to that the NACE is qualitatively proportional to the overlap between the hole and electron wavefunction as shown in Eq. (4). Though we only consider the minimal dimer model in our calculation, we expect that, in the thin film, aggregates larger than the dimer will further delocalize the wavefunction of holes and electrons and lead to a smaller NACE. The reduction of the prefactor C_l^2 will partially compensate for the increase in k_{nr} induced by the reduction in energy gap. It could account for the much smaller k_{nr} of CTA than that of iCT molecules with similar emission wavelength and molecular structure, and could be the underlying mechanism for the observation in the experiments where the k_{nr} shows even an anti-energy gap law behaviour through the formation of molecular aggregates with a strong xCT [24]. The similar effect has been discussed in organic solar cells where the electron-hole separation and delocalization in the donor-acceptor interface will reduce the nonadiabatic coupling and hence suppress the non-radiative decay process [36]. We also calculated the reorganization energy (λ) of monomers and dimers (Figure S12). In ω>1,000 cm^{-1}, λ of dimers is 862.4 cm^{-1}, which is slightly larger than that of monomers (699.5 cm^{-1}).

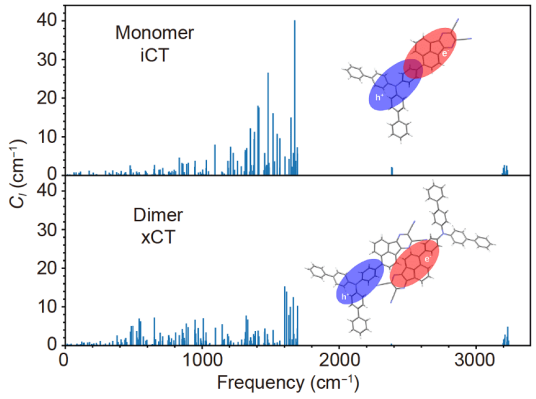

Figure 6 The prefactor C_l of k_m in Eq. (1) for the dpTPAAP monomer and dimer **1** at their optimized S_0 structures (color online).

2.7 Device performances

To evaluate the electroluminescent performance of dpTPAAP, some OLEDs were fabricated with multilayer configurations of indium tin oxide (ITO)/1,4,5,8,9,11-hexaazatriphenylenehexacarbonitrile (HATCN, 5 nm, hole-injecting layer)/*N*,*N*′-bis(naphthalen-1-yl)-*N*,*N*′-bis(phenyl) benzidine (NPB, 70 nm, hole transporting layer)/4,4′,4″-tris (carbazol-9-yl)triphenylamine (TCTA, 10 nm, exciton blocking layer)/TPBi: *x* wt.% dpTPAAP (30 nm, emitting layer)/TPBi (60 nm, electron transporting layer)/LiF (1 nm, electron-injecting layer)/Al (150 nm) (device A: *x* = 1, de-

vice B: x = 5, device C: x = 15 and device D: x = 30). As depicted in Figure 7 and Table S5, device A demonstrated intense DR emission with peak wavelength at 675 nm. As the increase of doping concentrations, the EL spectra of the devices red-shift and fall into NIR region with peak wavelengths at 710, 730 and 752 nm for devices B, C and D, respectively. In addition to the widely-tunable EL by a simple doping-concentration control, device A, B, C and D based on the dpTPAAP achieved high maximum EQEs of 24.8%, 17.0%, 13.0% and 6.8%, respectively, which are among the best results for DR and NIR OLEDs based on TADF emitters [24,29,32–40]. Importantly, the NIR device B, C and D exhibited high radiant emittances of 69.06, 86.02 and 78.36 W m^{-2}, respectively. As the increase of doping concentration, the turn-on voltage decrease from 3.0 V for device A to 2.6 V for device B and to 2.5 V for device C and D, which could be ascribed to the trap-assisted recombination on the dopants at the high doping concentration. In addition, devices with higher doping concentration demonstrate a more rapid increase of current density (J) as the increase of voltage, which could be ascribed to the better carrier injection and the formation of percolative charge transport on dopants [41]. As the increase of doping concentration in the emitting layer, devices show alleviated efficiency roll-offs, which could be ascribed to the shortened delayed fluorescence lifetimes for doped films with higher doping concentration [24], thus reducing the exciton-exciton annihilation and exciton-polaron annihilation at high current density [42,43]. For comparison, device E based on dpTPAAZ was also fabricated with a configuration of ITO/HATCN (5 nm)/NPB (70 nm)/TCTA (10 nm)/5 wt.%-doped dpTPAAZ:TPBi (30 nm)/TPBi (60 nm)/LiF (1 nm)/Al (150 nm). Device E demonstrates NIR emission with peak wavelength at 757 nm, which is close to EL the peak of device D based on the 30 wt.%-doped dpTPAAP:TPBi film. Nevertheless, the maximum EQE of device E is only 1.2% due to the low PLQY of the emitting layer, which is much lower than that of device D. Although, with nearly the same emission peak, the much higher EQE of device D than device E suggests the superiority of CTA in achieving high-efficiency NIR EL.

3 Conclusions

In this work, we have presented that the suppression of electronic nonadiabatic coupling is a novel approach for organic emissive materials to suppress the non-radiative decay processes and overcome the energy gap law. Also, a feasible strategy was developed to reduce the electronic nonadiabatic coupling by forming CTA for organic materials to achieve high-efficiency NIR emissions. The developed

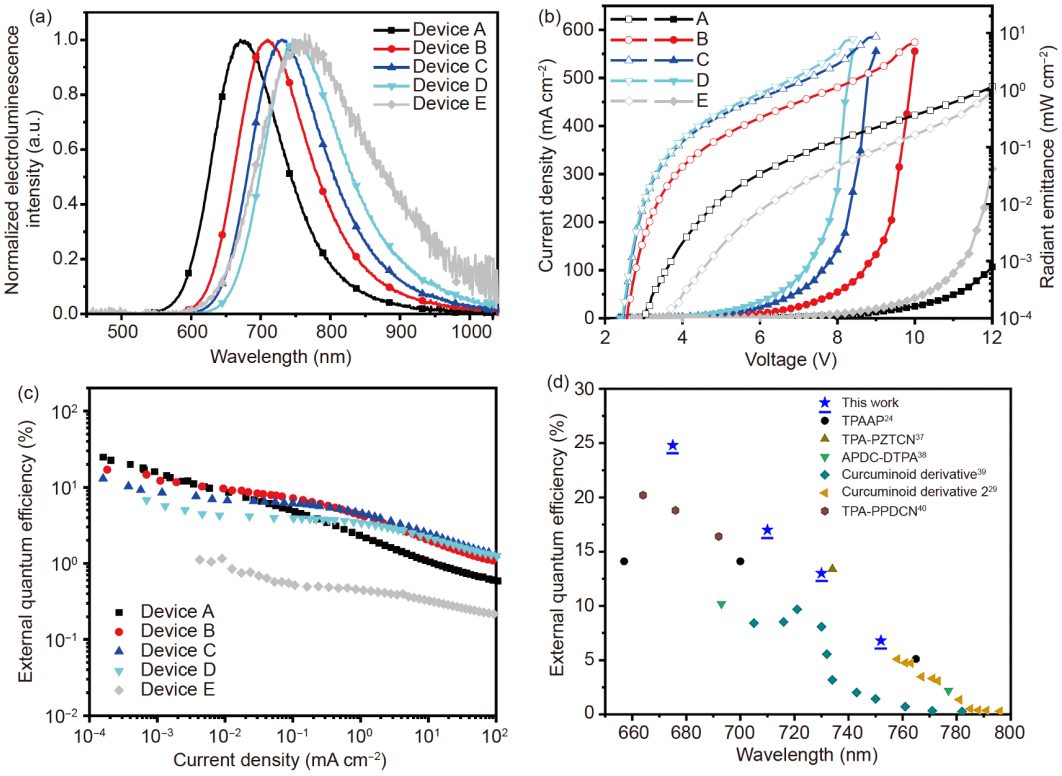

Figure 7 (a) Electroluminescence spectra recorded at the current of 1 mA cm^{-2} for device A, B, C, D and E. (b) Current density-voltage-radiant emittance characteristics for device A, B, C, D and E. (c) EQE as a function of current density. (d) Maximum EQE summary of the representative deep-red and NIR OLEDs based on TADF emitters with emission peaks from 650 to 800 nm (color online).

dpTPAAP molecules, through forming CTA, exhibit widely-tunable emissions from 621 to 802 nm with high PLQYs of over 80% in NIR region. Importantly, in comparison with iCT molecules with similar molecular structure and NIR emission around 760 nm, the CTA emitter displays a 6.5 times higher PLQY contributed by a 3.8 times smaller k_{nr}. Theoretical investigations reveal that the formation of CTA with the involvement of xCT in the excited states can suppress nonadiabatic coupling, thus alleviating the limitation of energy gap law. The formation of CTA is well verified by the absorption spectra and EPR measurements and rationalized by quantum chemical calculations. The OLEDs fabricated with the CTA emitter exhibited high-efficiency DR and NIR EL. The mechanism illustrated by the theoretical investigations would shed light on the photophysical behaviours of CT emitters and provide a novel approach for organic materials to overcome the energy gap law. It is anticipated that our work paves a superior way for the rational design of high-efficiency NIR organic materials, and lays a foundation for the applications of CTA for a wide variety of fields.

Acknowledgements This work was supported by the National Natural Science Foundation of China (51773109, 21788102), National Key R&D Program of China (2020YFA0715001, 2017YFA0204501), National Postdoctoral Program for Innovative Talents (BX20180159), and the Project funded by China Postdoctoral Science Foundation (2019M660606). Research presented in this article was posted on a preprint server prior to publication in Science China Chemistry. The corresponding preprint article can be found here: https://doi.org/10.26434/chemrxiv.14330591.v1.

Conflict of interest The authors declare no conflict of interest.

Supporting information The supporting information is available online at http://chem.scichina.com and http://link.springer.com/journal/11426. The supporting materials are published as submitted, without typesetting or editing. The responsibility for scientific accuracy and content remains entirely with the authors.

1 Bünzli JCG, Eliseeva SV. *J Rare Earths*, 2010, 28: 824–842
2 Kenry , Duan Y, Liu B. *Adv Mater*, 2018, 30: 1802394
3 Qian G, Wang ZY. *Chem Asian J*, 2010, 5: 1006–1029
4 Zampetti A, Minotto A, Cacialli F. *Adv Funct Mater*, 2019, 29: 1807623
5 Chen S, Weitemier AZ, Zeng X, He L, Wang X, Tao Y, Huang AJY, Hashimotodani Y, Kano M, Iwasaki H, Parajuli LK, Okabe S, Teh DBL, All AH, Tsutsui-Kimura I, Tanaka KF, Liu X, McHugh TJ. *Science*, 2018, 359: 679–684
6 Khan Y, Han D, Pierre A, Ting J, Wang X, Lochner CM, Bovo G, Yaacobi-Gross N, Newsome C, Wilson R, Arias AC. *Proc Natl Acad Sci USA*, 2018, 115: E11015
7 Yamanaka T, Nakanotani H, Hara S, Hirohata T, Adachi C. *Appl Phys Express*, 2017, 10: 074101
8 Jeon Y, Choi HR, Kwon JH, Choi S, Nam KM, Park KC, Choi KC. *Light Sci Appl*, 2019, 8: 114
9 Khan Y, Han D, Ting J, Ahmed M, Nagisetty R, Arias AC. *IEEE Access*, 2019, 7: 128114
10 Siebrand W. *J Chem Phys*, 1967, 46: 440–447
11 Englman R, Jortner J. *Mol Phys*, 1970, 18: 145–164
12 Yao L, Zhang S, Wang R, Li W, Shen F, Yang B, Ma Y. *Angew Chem Int Ed*, 2014, 53: 2119–2123
13 Wang S, Yan X, Cheng Z, Zhang H, Liu Y, Wang Y. *Angew Chem Int Ed*, 2015, 54: 13068–13072
14 Peng Q, Obolda A, Zhang M, Li F. *Angew Chem Int Ed*, 2015, 54: 7091–7095
15 Ai X, Evans EW, Dong S, Gillett AJ, Guo H, Chen Y, Hele TJH, Friend RH, Li F. *Nature*, 2018, 563: 536–540
16 Deng C, Niu Y, Peng Q, Qin A, Shuai Z, Tang BZ. *J Chem Phys*, 2011, 135: 014304
17 Metcalfe J, Phillips D. *J Chem Soc Faraday Trans 2*, 1976, 72: 1574–1583
18 Siebrand W, Williams DF. *J Chem Phys*, 1968, 49: 1860–1871
19 Yang J, Chi Z, Zhu W, Tang BZ, Li Z. *Sci China Chem*, 2019, 62: 1090–1098
20 Wu Q, Deng C, Peng Q, Niu Y, Shuai Z. *J Comput Chem*, 2012, 33: 1862–1869
21 Chen WC, Chou PT, Cheng YC. *J Phys Chem C*, 2019, 123: 10225–10236
22 Wei YC, Wang SF, Hu Y, Liao LS, Chen DG, Chang KH, Wang CW, Liu SH, Chan WH, Liao JL, Hung WY, Wang TH, Chen PT, Hsu HF, Chi Y, Chou PT. *Nat Photonics*, 2020, 14: 570–577
23 Chernyak V, Mukamel S. *J Chem Phys*, 2000, 112: 3572–3579
24 Xue J, Liang Q, Wang R, Hou J, Li W, Peng Q, Shuai Z, Qiao J. *Adv Mater*, 2019, 31: 1808242
25 Hirata S, Sakai Y, Masui K, Tanaka H, Lee SY, Nomura H, Nakamura N, Yasumatsu M, Nakanotani H, Zhang Q, Shizu K, Miyazaki H, Adachi C. *Nat Mater*, 2014, 14: 330–336
26 Zhang Q, Kuwabara H, Potscavage Jr. WJ, Huang S, Hatae Y, Shibata T, Adachi C. *J Am Chem Soc*, 2014, 136: 18070–18081
27 Chen WC, Huang B, Ni SF, Xiong Y, Rogach AL, Wan Y, Shen D, Yuan Y, Chen JX, Lo MF, Cao C, Zhu ZL, Wang Y, Wang P, Liao LS, Lee CS. *Adv Funct Mater*, 2019, 29: 1903112
28 Liang Q, Xu J, Xue J, Qiao J. *Chem Commun*, 2020, 56: 8988–8991
29 Ye H, Kim DH, Chen X, Sandanayaka ASD, Kim JU, Zaborova E, Canard G, Tsuchiya Y, Choi EY, Wu JW, Fages F, Bredas JL, D'Aléo A, Ribierre JC, Adachi C. *Chem Mater*, 2018, 30: 6702–6710
30 Madigan CF, Bulović V. *Phys Rev Lett*, 2003, 91: 247403
31 Wang M, Huang YH, Lin KS, Yeh TH, Duan J, Ko TY, Liu SW, Wong KT, Hu B. *Adv Mater*, 2019, 31: 1904114
32 Kronik L, Kümmel S. *Adv Mater*, 2018, 30: 1706560
33 Shao Y, Gan Z, Epifanovsky E, Gilbert ATB, Wormit M, Kussmann J, Lange AW, Behn A, Deng J, Feng X, Ghosh D, Goldey M, Horn PR, Jacobson LD, Kaliman I, Khaliullin RZ, Kuś T, Landau A, Liu J, Proynov EI, Rhee YM, Richard RM, Rohrdanz MA, Steele RP, Sundstrom EJ, Woodcock Iii HL, Zimmerman PM, Zuev D, Albrecht B, Alguire E, Austin B, Beran GJO, Bernard YA, Berquist E, Brandhorst K, Bravaya KB, Brown ST, Casanova D, Chang CM, Chen Y, Chien SH, Closser KD, Crittenden DL, Diedenhofen M, DiStasio Jr. RA, Do H, Dutoi AD, Edgar RG, Fatehi S, Fusti-Molnar L, Ghysels A, Golubeva-Zadorozhnaya A, Gomes J, Hanson-Heine MWD, Harbach PHP, Hauser AW, Hohenstein EG, Holden ZC, Jagau TC, Ji H, Kaduk B, Khistyaev K, Kim J, Kim J, King RA, Klunzinger P, Kosenkov D, Kowalczyk T, Krauter CM, Lao KU, Laurent AD, Lawler KV, Levchenko SV, Lin CY, Liu F, Livshits E, Lochan RC, Luenser A, Manohar P, Manzer SF, Mao SP, Mardirossian N, Marenich AV, Maurer SA, Mayhall NJ, Neuscamman E, Oana CM, Olivares-Amaya R, O'Neill DP, Parkhill JA, Perrine TM, Peverati R, Prociuk A, Rehn DR, Rosta E, Russ NJ, Sharada SM, Sharma S, Small DW, Sodt A, Stein T, Stück D, Su YC, Thom AJW, Tsuchimochi T, Vanovschi V, Vogt L, Vydrov O, Wang T, Watson MA, Wenzel J, White A, Williams CF, Yang J, Yeganeh S, Yost SR, You ZQ, Zhang IY, Zhang X, Zhao Y, Brooks BR, Chan GKL, Chipman DM, Cramer CJ, Goddard Iii WA, Gordon MS, Hehre WJ, Klamt A, Schaefer Iii HF, Schmidt MW, Sherrill CD, Truhlar DG, Warshel A, Xu X, Aspuru-Guzik A, Baer R, Bell AT, Besley NA, Chai JD, Dreuw A, Dunietz BD, Furlani TR, Gwaltney SR, Hsu CP, Jung Y, Kong J, Lambrecht DS, Liang WZ, Ochsenfeld C, Rassolov VA, Slipchenko LV, Subotnik JE, Van Voorhis T, Herbert JM, Krylov AI, Gill PMW, Head-Gordon M. *Mol*

Phys, 2015, 113: 184–215
34 Lu T, Chen F. *J Comput Chem*, 2012, 33: 580–592
35 Biswas S, Pramanik A, Pal S, Sarkar P. *J Phys Chem C*, 2017, 121: 2574–2587
36 Chen XK, Ravva MK, Li H, Ryno SM, Brédas JL. *Adv Energy Mater*, 2016, 6: 1601325
37 Balijapalli U, Nagata R, Yamada N, Nakanotani H, Tanaka M, D'Aléo A, Placide V, Mamada M, Tsuchiya Y, Adachi C. *Angew Chem Int Ed*, 2021, 60: 8477–8482
38 Yuan Y, Hu Y, Zhang YX, Lin JD, Wang YK, Jiang ZQ, Liao LS, Lee ST. *Adv Funct Mater*, 2017, 27: 1700986
39 Kim DH, D'Aléo A, Chen XK, Sandanayaka ADS, Yao D, Zhao L, Komino T, Zaborova E, Canard G, Tsuchiya Y, Choi E, Wu JW, Fages F, Brédas JL, Ribierre JC, Adachi C. *Nat Photon*, 2018, 12: 98–104
40 Yang T, Liang B, Cheng Z, Li C, Lu G, Wang Y. *J Phys Chem C*, 2019, 123: 18585–18592
41 Li C, Duan L, Li H, Qiu Y. *Org Electron*, 2013, 14: 3312–3317
42 Murawski C, Leo K, Gather MC. *Adv Mater*, 2013, 25: 6801–6827
43 Hasan M, Shukla A, Ahmad V, Sobus J, Bencheikh F, McGregor SKM, Mamada M, Adachi C, Lo SC, Namdas EB. *Adv Funct Mater*, 2020, 30: 2000580